UNSYS digital

The Journal of Instrumentation, Automation and Systems

Preliminary Study on Stability of a Hovering Bi-flap Flapping Wing Platform using Cycle-Averaged Linear Models

Woei Leong Chan†§, Muhammad Azli Bin Jaffar†, and Quoc Viet Nguyen§

†Mechanical Engineering Department, National University of Singapore, Singapore

§Temasek Laboratories, National University of Singapore, Singapore

Abstract—A preliminary study on the stability of a bi-flap flapping wing hovering platform is presented in this paper. The work includes the derivation of cycle-average linear longitudinal and lateral models, the experiment to determine the stability derivatives, and analysis on the identified system matrices. Also discussed in the paper is the validity of using a cycle-averaged model to represent the dynamics of the flapping wing platform, and the validity of using small perturbation theory to linearize the nonlinear model. Results show that the platform is unstable longitudinally and laterally about the hovering equilibrium. Longitudinally, the natural modes are short period unstable oscillatory mode, fast subsidence mode, and slow divergent mode. Laterally, the natural modes are neutral mode, fast subsidence mode, and long period unstable oscillatory mode.

Keywords—Cycle-averaged model, bi-flap, flapping wing, stability.

I. Introduction

FLAPPING wing flying vehicles have gained a significant amount of interest in recent days due to its bio-mimicry features and relatively high efficiency in low Reynolds number region due to the utilization of unsteady aerodynamics. Over the years, many people have tried to derive the nonlinear model of flapping wing flight. Nonlinear models and even flight control strategies were proposed by various parties, such as Doman *et al.* [1], Deng *et al.* [2], Khan and Agrawal [3], Sun *et al.* [4]. Albeit the advantage of representing the real system more accurately, nonlinear models are usually complex and come with various forms which do not allow the usage of common tools to analyze stability. What is lacking is a common model form and common methodology to serve as a common ground of comparison. This is easily achievable by using linear models.

Under quasi-static assumption, the dynamic of flapping wing may be treated as a rigid body system which will allow it to be represented by linear models about certain equilibrium points. Taylor and Thomas [5] are among the first to introduce this concept for insect flight dynamics study. The idea was also adopted by Sun *et al.* [6][7] to derive the longitudinal and lateral linear models of bumblebee, and did an in depth analysis on the insect flight dynamics. As a matter of fact, most in depth studies on flapping wing stability uses linear model or small perturbation excitation, such as Gao *et al*. [8][9], Faruque and Humbert [10][11], and Zhang and Sun [12]. Most of the studies were aided by computational fluid dynamics (CFD) due to the challenge of identifying the stability derivatives using experimental techniques.

This paper is about the preliminary study on the stability of the Svari flapping wing platform. It is the brainchild of a team of undergraduate third year students from the Mechanical Engineering Department of the National University of Singapore. It is a bi-flap flapping wing platform similar to the DelFly [13], but it was designed to be a hovering platform with the capability to take off from a standing position on its empennage.

The present work is focused on preliminary analysis on stability using cycle-averaged linear models. The motivation is to pave the road to better understanding of the stability issue of flapping wing flying vehicle, and the subsequent implementation of automatic flight control. The paper is organized as follows. Section II will be elaborating the details of Svari platform. The flapping wing platform dynamic models are described in Section III. The originally nonlinear model is being separated into the longitudinal and lateral linear models under certain assumptions. The experimental setup to acquire the stability derivatives is presented in Section IV. Section V presents the result and discussion. Finally, the concluding remarks end the paper.

II. SVARI Platform

A. Flapping Mechanism & Gearbox

The flapping mechanism is designed based on a four bar linkage crank-rocker system. **Figure 1** shows the flapping mechanism. Two synchronized crank-rocker systems drive the crossed struts. Each strut holds the wings on both left and right sides. The mechanism allows the wings to clap and fling on the left and right sides at the end of clap stroke (upstroke).

Corresponding author: Woei Leong Chan (e-mail: tslcwl@nus.edu.sg).
This paper was submitted on September 29, 2014; revised on October 29, 2014; and accepted on November 11, 2014.

The gear ratio is 22.22:1. The maximum angle ($\Phi_{\max}$) and minimum angle ($\Phi_{\min}$) between the upper strut and lower strut flapping in opposite phase is 73.26°, and 12.58°, respectively. Thus the flapping stroke angle is 60.68°. Mean stroke angle ($\overline{\phi_f}$) is 10° shifted to the dorsal side (upper side) of the platform. The length of the crank-rocker components are: l_0 = 17.09mm, l_1 = 2.3mm, l_2 = 13mm, l_3 = 9mm. **Figure 2** shows the ideal stroke angles, and stroke amplitude under no load condition. As shown in the figure, the fling stroke (downstroke) is slightly shorter than the clap stroke (upstroke). The upper wing and the lower wing stroke angles ($\phi_{f,u}$ and $\phi_{f,l}$) are symmetrical about the mean stroke angle of 10°. The motor is the HobbyKing AP03 brushless motor.

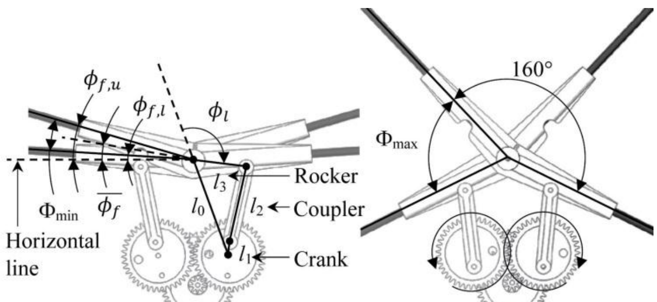

Figure 1 Gearbox and flapping mechanism

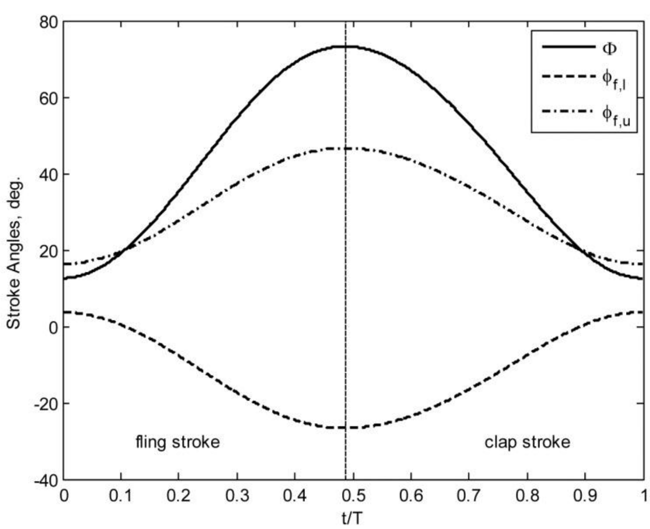

Figure 2 Ideal stroke angles under no load condition

B. *Dimension & Mass Properties*

The Svari platform has a total mass (m) of 0.05535kg (55.35 g). The moment of inertia (I_x, I_y, I_z) about the body axes are determined using computer aided design (CAD) software. Each component is drawn as accurate as possible in the CAD software to match its physical mass. The density of each component is assumed to be evenly distributed. The identified moments of inertia are $I_x =$ 4.7079×10^{-4}kg·m^2, $I_y =$ 1.7400×10^{-4}kg·m^2, $I_z =$ 4.1176×10^{-4}kg·m^2.

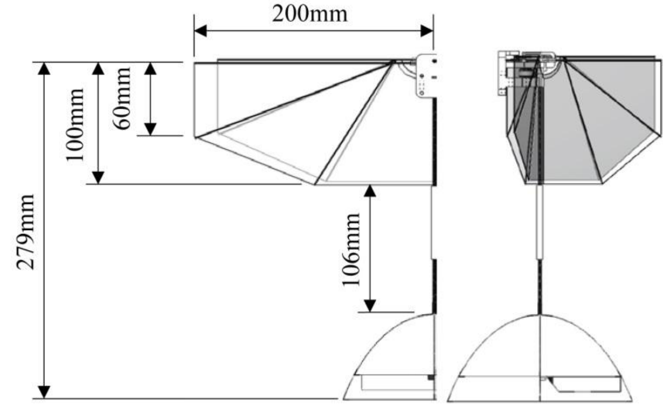

Figure 3 Svari dimension

As shown in **Figure 3**, the Svari platform is 279mm in height, wing span (b) is 400mm, and the distance between the trailing edge of the wing to the leading edge of the tail is 106mm. The mean aerodynamic chord ($\bar{c}$) is 0.09m, and total wing area (S_w) is 0.06916m^2. The horizontal and vertical tails have the same area (S_t) of 0.00453m^2.

III. Dynamic Model

A. *Coordinate Systems*

The Equations of Motion (EOM) are to be derived around the Body-Fixed Coordinate System ($OX_BY_BZ_B$) originated at the center of gravity (CG) of the flying vehicle. The body-fixed frame moves together with flying vehicle. The X_B–axis points towards the front of the vehicle, Y_B–axis points towards the left, and Z_B–axis points downwards, parallel to the tail as shown in **Figure 4**. **Figure 4** also shows the Local Horizontal Coordinate System ($OX_HY_HZ_H$). Similarly, the origin is the CG of the vehicle, the X_HY_H-plane is always horizontal with X_H always points to the North, and Z_H points to the direction of gravitation pull. The three angles shown in the figure are called the Euler angles. They are also called the roll angle (ϕ), the pitch angle (θ), and the yaw angle (ψ). These angles define the attitude of the body relative to North and local horizontal plane. The forces and moments discussed in the subsequent sections are forces and moments as observed on the Body-Fixed Coordinate System.

B. *Equations of Motion*

The EOM consist of the force equations, the moment equations, and kinematics equations. These equations are listed as Eq. 1 to 3, respectively.

$$\begin{aligned} \dot{u} &= X/m + rv - qw - g\sin\theta \\ \dot{v} &= Y/m + pw - ru + g\cos\theta\sin\phi \\ \dot{w} &= Z/m + qu - pv + g\cos\theta\cos\phi \end{aligned} \tag{1}$$

$$\begin{aligned} L &= I_x\dot{p} + (I_z - I_y)qr - I_{xz}(\dot{r} + pq) \\ M &= I_y\dot{q} + (I_x - I_z)pr - I_{xz}(r^2 - p^2) \\ N &= I_z\dot{r} + (I_y - I_x)pq - I_{xz}(\dot{p} - qr) \end{aligned} \tag{2}$$

$$\dot{\phi} = p + (q \sin\phi + r\cos\phi)\tan\theta$$
$$\dot{\theta} = q\cos\phi - r\sin\phi \quad (3)$$
$$\dot{\psi} = (q\sin\phi + r\cos\phi)\ \sec\theta$$

The nonlinear EOM is derived for rigid body. $\{X, Y, Z\}$, $\{L, M, N\}$, $\{u, v, w\}$, and $\{p, q, r\}$ are the force, moment, translational velocity and angular rate components on the Body-Fixed Coordinate System. Mass (m), components of the moment of inertia (I_x, I_y, I_z, I_{xz}) and gravitational accleration (g) are constant. Force equations govern the effect of force on a body. Likewise, moment equations govern the effect of moment on a body. The kinematic equations describe the change of the Euler angles due to the body frame angular velocities. Detail derivation is available in Nelson's [14].

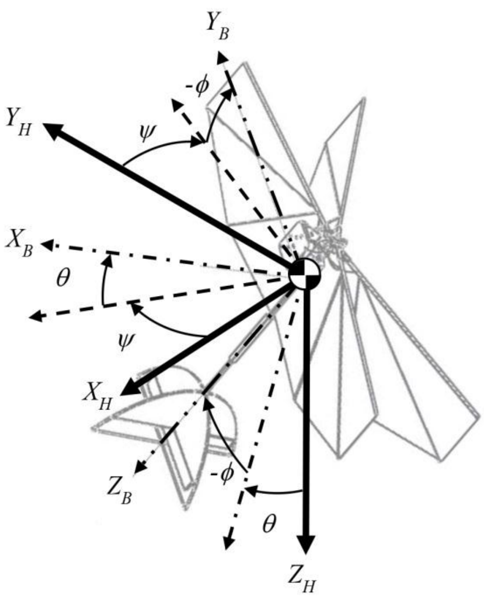

Figure 4 Coordinate systems originated at CG & Euler angles

C. *Cycle-Averaged Model*

In order to use Eq. 1 to 3 for flapping wing analysis, the flapping wing body is assumed to be rigid. Cycle-averaged model is a model based on quasi-static approximation. It is commonly used in analysis of helicopter dynamics and fixed wing aircraft with high aeroelasticity as mentioned by Taylor & Thomas [5]. As claimed by Taylor and Thomas, for the flapping wing case, the dynamic change of force due to the flapping motion could be coupled with the platform motion's natural mode, but if the flapping frequency is at least ten times the platform's natural frequency, quasi-static approximation should work well and the assumption of rigid body should hold.

D. *Linearization of Longitudinal Model*

Nelson [14] presented the detail derivation of the linearization of aircraft dynamic models. Similar idea is applied here although some assumptions are not exactly the same due to the difference of flapping wing and fixed-wing vehicles, but the outcome is similar. Do note that this paper is trying to derive a cycle-averaged linear model of hovering flight. Small perturbation theory is used whereby it is assumed that the forces and moments are generated by small perturbation of the state variables and control surfaces about an equilibrium state. In our case, the equilibrium state is steady hovering where lift equals to the weight, and the sum of all other forces and moments are zeroes. More importantly, since the perturbations are small, it is assumed that the effects are linear. The state variables that are contributing to the forces and moments are the translational velocities, and angular velocities. Other than that, the elevator and rudder deflections (δ_e, δ_r) contribute as well. Similar to aircraft dynamics, the model is separated into longitudinal and lateral models. Eq. 4 shows the linear model of the longitudinal forces and moments. The "Δ" indicates small perturbation.

$$\begin{aligned}
\Delta X &= \frac{\partial X}{\partial u}\Delta u + \frac{\partial X}{\partial w}\Delta w + \frac{\partial X}{\partial q}\Delta q + \frac{\partial X}{\partial \delta_e}\Delta\delta_e + \frac{\partial X}{\partial f}\Delta f \\
\Delta Z &= \frac{\partial Z}{\partial u}\Delta u + \frac{\partial Z}{\partial w}\Delta w + \frac{\partial Z}{\partial q}\Delta q + \frac{\partial Z}{\partial \delta_e}\Delta\delta_e + \frac{\partial Z}{\partial f}\Delta f \qquad (4)\\
\Delta M &= \frac{\partial M}{\partial u}\Delta u + \frac{\partial M}{\partial w}\Delta w + \frac{\partial M}{\partial q}\Delta q + \frac{\partial M}{\partial \delta_e}\Delta\delta_e + \frac{\partial M}{\partial f}\Delta f
\end{aligned}$$

Applying small perturbation theory on the longitudinal equations of Eq. 1 to Eq. 3, and neglecting the products of the disturbances due to their small values:

$$\begin{aligned}
\Delta\dot{u} &= \Delta X/m - g\Delta\theta \\
\Delta\dot{w} &= \Delta Z/m + g \qquad (5)\\
\Delta\dot{q} &= \Delta M/I_y \\
\Delta\dot{\theta} &= q
\end{aligned}$$

The rate derivatives are extremely difficult to obtain by experimental means. Thus, for this preliminary study, the rate derivatives are neglected. Substituting Eq. 4 in to Eq. 5 yields the cycle-averaged linear longitudinal model:

$$\begin{bmatrix}\Delta\dot{u}\\ \Delta\dot{w}\\ \Delta\dot{q}\\ \Delta\dot{\theta}\end{bmatrix} = \boldsymbol{A}_{lon}\begin{bmatrix}\Delta u\\ \Delta w\\ \Delta q\\ \Delta\theta\end{bmatrix} + \boldsymbol{B}_{lon}\begin{bmatrix}\Delta\delta_e\\ \Delta f\end{bmatrix} \qquad (6)$$

where $\boldsymbol{A}_{lon} = \begin{bmatrix} X_u & X_w & 0 & -g\\ Z_u & Z_w & 0 & 0\\ M_u & M_w & 0 & 0\\ 0 & 0 & 1 & 0\end{bmatrix}$, $\boldsymbol{B}_{lon} = \begin{bmatrix} X_{\delta_e} & X_f\\ Z_{\delta_e} & Z_f\\ M_{\delta_e} & M_f\\ 0 & 0\end{bmatrix}$

$$X_u = \partial X/\partial u \cdot 1/m,\ X_w = \partial X/\partial w \cdot 1/m$$
$$X_{\delta_e} = \partial X/\partial \delta_e \cdot 1/m,\quad X_f = \partial X/\partial f \cdot 1/m$$
$$Z_u = \partial Z/\partial u \cdot 1/m,\ \ Z_w = \partial Z/\partial w \cdot 1/m$$
$$Z_{\delta_e} = \partial Z/\partial \delta_e \cdot 1/m,\quad Z_f = \partial Z/\partial f \cdot 1/m$$
$$M_u = \partial M/\partial u \cdot 1/I_y,\ M_w = \partial M/\partial w \cdot 1/I_y$$
$$M_{\delta_e} = \partial M/\partial \delta_e \cdot 1/I_y,\quad M_f = \partial M/\partial f \cdot 1/I_y$$

X_k, Z_k, and M_k are the forward force, downward force, and pitching moment derivatives due to variable k. Do note that the control derivatives are not identified because they are not needed for stability analysis.

E. Linearization of Lateral Model

Similar to the longitudinal model, the lateral model can be derived using small perturbation theory as followings:

$$\begin{aligned}\Delta Y &= \frac{\partial Y}{\partial v}\Delta v + \frac{\partial Y}{\partial p}\Delta p + \frac{\partial Y}{\partial r}\Delta r + \frac{\partial Y}{\partial \delta_r}\Delta\delta_r \\ \Delta L &= \frac{\partial L}{\partial v}\Delta v + \frac{\partial L}{\partial p}\Delta p + \frac{\partial L}{\partial r}\Delta r + \frac{\partial L}{\partial \delta_r}\Delta\delta_r \\ \Delta N &= \frac{\partial N}{\partial v}\Delta v + \frac{\partial N}{\partial p}\Delta p + \frac{\partial N}{\partial r}\Delta r + \frac{\partial N}{\partial \delta_r}\Delta\delta_r\end{aligned} \quad (7)$$

The products of the disturbances in Eq. 1 to 3, are neglected. Furthermore, $I_x \gg I_{xz}$ and $I_z \gg I_{xz}$ for the vehicle configuration:

$$\begin{aligned}\Delta\dot{v} &= \Delta Y/m + g\Delta\phi \\ \Delta\dot{p} &= \Delta L/I_x \\ \Delta\dot{r} &= \Delta N/I_z \\ \Delta\dot{\phi} &= p\end{aligned} \quad (8)$$

Similar to the longitudinal model, the rate derivatives are neglected. Substituting Eq. 7 in to Eq. 8 yields the cycle-averaged linear lateral model:

$$\begin{bmatrix}\Delta\dot{v}\\ \Delta\dot{p}\\ \Delta\dot{r}\\ \Delta\dot{\phi}\end{bmatrix} = \boldsymbol{A}_{lat}\begin{bmatrix}\Delta v\\ \Delta p\\ \Delta r\\ \Delta\phi\end{bmatrix} + \boldsymbol{B}_{lat}\Delta\delta_r \quad (9)$$

where $\boldsymbol{A}_{lat} = \begin{bmatrix}Y_v & 0 & 0 & g\\ L_v & 0 & 0 & 0\\ N_v & 0 & 0 & 0\\ 0 & 1 & 0 & 0\end{bmatrix}$, $\boldsymbol{B}_{lat} = \begin{bmatrix}Y_{\delta_r}\\ L_{\delta_r}\\ N_{\delta_r}\\ 0\end{bmatrix}$

$$Y_v = \partial Y/\partial v \cdot 1/m,\ Y_{\delta_r} = \partial Y/\partial \delta_r \cdot 1/m$$

$$L_v = \partial L/\partial v \cdot 1/I_x,\ L_{\delta_r} = \partial L/\partial \delta_r \cdot 1/I_x$$

$$N_v = \partial N/\partial v \cdot 1/I_z,\ N_{\delta_r} = \partial N/\partial \delta_r \cdot 1/I_z$$

Y_k, L_k, and N_k are the sideward force, rolling moment, and yawing moment derivatives corresponding to variable k. Do note that the control derivatives are not identified because they are not needed for stability analysis.

IV. Experimental Setup

Experiment was conducted to determine the derivatives in Eq. 6 and Eq. 9. The Svari platform was mounted on an ATI Nano17 load cell. The load cell measures 3-axes forces and 3-axes moments. A low pass filter was applied to filter out the high frequency noise. Then, the data were transformed to the Body-Fixed Coordinate System. Subsequently, the data of at least five cycles were averaged to obtain the cycle-average data. The cycle-averaged data of equilibrium were then deducted from the cycle-averaged data of the various cases to obtain the small perturbation of forces and moments.

Figure 5 shows the close-up look of the experimental setup. The Svari platform was installed on the load cell mounted on a stand. A Neodymium magnet was installed on one of the gears, and a Hall Effect switch was used to monitor the flapping frequency. The setup was installed in a closed-loop wind tunnel with H600mm × W600mm × L2000mm test section. The Svari platform was oriented in various configurations to simulate the u, v, and w velocities as shown in **Figure 6**.

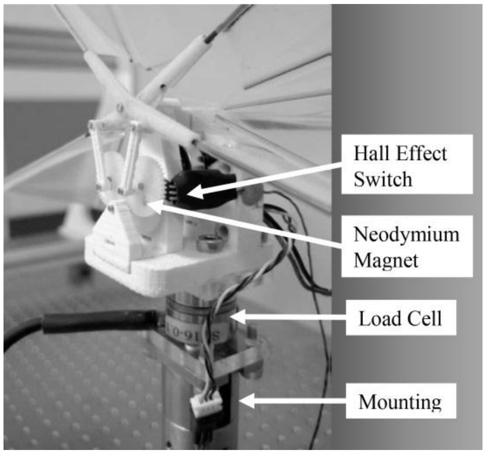

Figure 5 Close-up look of the experimental setup

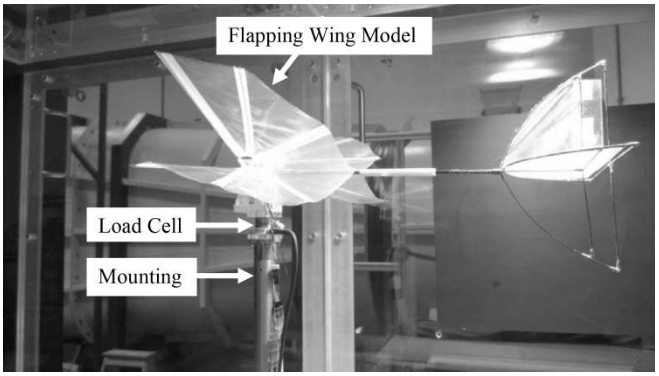

Figure 6(a) Experimental setup in the wind tunnel (*w*)

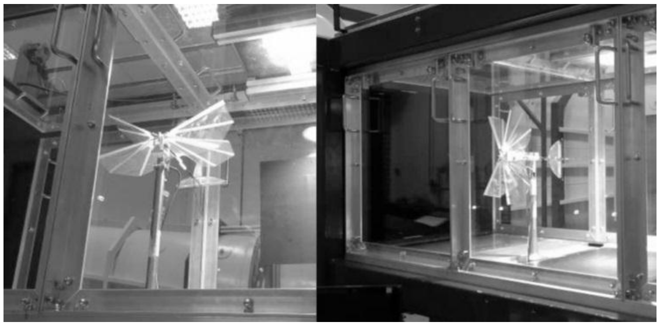

Figure 6(b) Experimental setup in the wind tunnel (*v* & *u*)

V. Result & Discussions

The gravitational acceleration (g) used in this paper is 9.81m/s^2. Hovering equilibrium of the Svari platform is u = 0m/s, v = 0m/s, w = 0m/s, p = 0rad/s, q = rad/s, r = 0rad/s, θ = 0rad, ϕ = 0rad. The flapping frequency (f) is 16Hz at the equilibrium condition.

A. Longitudinal Model and Stability

Figure 7 shows the effect of small downward velocity perturbation to the forces and moments. The derivatives can be determined by calculating the gradients of the linear curves. The gradients represent the amount of changes to the forces and moments with a unit change of downward velocity. The fact that the data can be fitted nicely into linear curves proves that the linearization using small perturbation theory on the longitudinal model of this platform is legitimate. However, the linear curves do not cross the origin by small margins, which mean the equilibrium is slightly off. It is assumed that the small margins can be compensated by the applying the control surfaces trim.

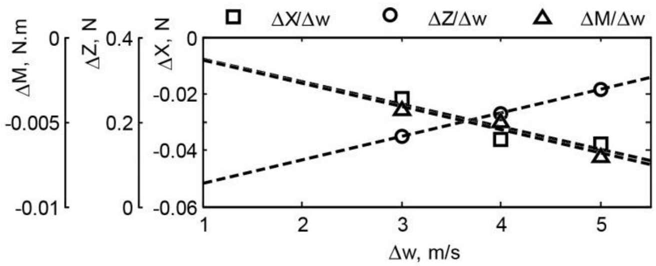

Figure 7 Changes of forces and moments due to small perturbation of *w*

TABLE I GRADIENTS OF LINEAR CURVES

	∂X	∂Z	∂M
∂u	0.2702	-0.1694	0.01248
∂w	-0.007950	0.05540	-0.001376

TABLE I lists down the gradients determined from the linear curves. From the table, forward velocity perturbation would induce forward force, increase lift, and generate pitch up moment. Downward velocity perturbation has lesser effect, but would still generate small amount of backward force, downward force, and pitch down moment.

Dividing the gradients by mass or moment of inertia and substituting the derivatives into the system matrix of Eq. 6, we have the longitudinal system matrix as follows:

$$\boldsymbol{A}_{lon} = \begin{bmatrix} 4.8817 & -0.1436 & 0 & -9.81 \\ -3.0605 & 1.0009 & 0 & 0 \\ 71.6954 & -7.9098 & 0 & 0 \\ 0 & 0 & 1 & 0 \end{bmatrix}$$

TABLE II lists down the eigenvalues of the system matrix. The longitudinal model has three modes:

Mode 1 (short period unstable oscillatory mode),

Mode 2 (fast subsidence mode), and

Mode 3 (slow divergent mode)

TABLE II EIGENVALUES OF THE LONGITUDINAL SYSTEM MATRIX

Mode 1, $\lambda_{lon,1,2}$	Mode 2, $\lambda_{lon,3}$	Mode 3, $\lambda_{lon,4}$
6.3215 ± 7.4078i	-7.4231	0.6626

TABLE III EIGENVECTORS OF THE LONGITUDINAL SYSTEM MATRIX

	Mode 1	Mode 2	Mode 3
Δu	0.0820 ± 0.1021i	0.1062	0.1098
Δw	-0.0439 ± 0.0024i	0.0386	0.9932
Δq	0.9852	-0.9847	0.0216
$\Delta \theta$	0.0657 ∓ 0.0770i	0.1327	0.0327

From the eigenvectors listed in **TABLE III**, Mode 1 and Mode 2 affect the pitch rate most, while Mode 3 affects downward velocity primarily. As indicated in **TABLE IV**, the short period unstable oscillatory mode takes only 0.11s to double its amplitude. That is only 1.76 times the flapping period, which means the amplitude of the state variables will be doubled in less than 2 flapping cycles. Its oscillation period is 0.85s, which indicates that the state variables oscillate at the period of 13.6 times the flapping period. It is called "short period" due to its shorter period compared to the oscillatory mode in the lateral dynamics. Fast subsidence mode takes 0.09s (1.44 flapping cycles) to reduce its amplitude by half, while the slow divergent mode takes 1.05s (16.8 flapping cycles) to double its amplitude. The following equations are used to determine the period (P) and $t_{\text{double/half}}$.

$$P = 2\pi/\omega \qquad (10)$$

$$t_{\text{double/half}} = 0.693/|\eta| \qquad (11)$$

where η = real part of eigenvalue

ω = imaginary part of eigenvalue

TABLE IV TIME CONSTANT OF THE LONGITUDINAL NATURAL MODES

Mode 1			Mode 2		Mode 3	
Stability	P	t_{double}	**Stability**	t_{half}	**Stability**	t_{double}
Unstable	0.85	0.11	Stable	0.09	Unstable	1.05

Do note that at any time, the system response is a superposition of all three modes. Thus, the Svari platform is unstable longitudinally about hovering equilibrium.

B. Lateral Model and Stability

Similar to the longitudinal case, **TABLE V** lists down the gradients determined from the linear curve of lateral case. From the table, positive sideward velocity perturbation generates negative sideward force, small amount of negative rolling moment, and negative yawing moment.

TABLE V GRADIENTS OF LINEAR CURVES

	∂Y	∂L	∂N
∂v	-0.1480	-0.005674	-0.005877

Dividing the gradients by mass or moment of inertia and substituting the derivatives into the system matrix of Eq. 9, we have the lateral system matrix as follows:

$$\boldsymbol{A}_{lat} = \begin{bmatrix} -2.6739 & 0 & 0 & 9.81 \\ -12.0517 & 0 & 0 & 0 \\ -14.2731 & 0 & 0 & 0 \\ 0 & 1 & 0 & 0 \end{bmatrix}$$

TABLE VI lists down the eigenvalues of the system matrix. The lateral model has three modes:

Mode 1 (neutral mode),

Mode 2 (fast subsidence mode), and

Mode 3 (long period unstable oscillatory mode).

TABLE VI EIGENVALUES OF THE LATERAL SYSTEM MATRIX

Mode 1, $\lambda_{lat,1}$	**Mode 2,** $\lambda_{lat,2}$	**Mode 3,** $\lambda_{lat,3,4}$
0	-6.2539	1.7900 ± 4.3801i

From the eigenvectors listed in **TABLE VII**, Mode 1 only affects roll rate, Mode 2 and Mode 3 affect roll and yaw primarily. As indicated in **TABLE VIII**, the fast subsidence mode takes only 0.11s (1.76 flapping cycles) to reduce the amplitude of the state variables by half. The long period unstable oscillatory mode takes 0.39s (6.24 flapping cycles) to double the state variables. Its oscillation period is 1.43s (22.88 flapping cycles). It is called "long period" due to its considerably longer period compared to the oscillatory mode in the longitudinal dynamics.

Due to the fact that the system response is a superposition of all three modes, the Svari platform is unstable laterally about hovering equilibrium.

TABLE VII EIGENVECTORS OF THE LATERAL SYSTEM MATRIX

	Mode 1	**Mode 2**	**Mode 3**
Δv	0	0.3154	-0.0918 ± 0.2246i
Δp	1	0.6077	0.6179
Δr	0	0.7197	0.7318
$\Delta \phi$	0	-0.1151	0.0585 ± 0.1432i

TABLE VIII TIME CONSTANT OF THE LATERAL NATURAL MODES

Mode 1	**Mode 2**		**Mode 3**		
Stability	**Stability**	t_{half}	**Stability**	P	t_{double}
Neutral	Stable	0.11	Unstable	1.43	0.39

C. Validity of Cycle-Averaged Model

From the force and moment measurement which fit nicely to linear curves, it is proven that the use of small perturbation theory for linearization is legitimate, but the validity of cycle-averaged model is yet to be proven. It can be done by comparing the flapping frequency and the frequencies of the natural modes. From the eigenvalues of the system matrices, the natural frequencies of the Svari platform can be calculated as $\omega/2\pi$. **TABLE IX** lists down the natural frequencies and the flapping frequency.

TABLE IX FREQUENCIES OF FLAPPING AND NATURAL MODES

Flapping Frequency	**Longitudinal Oscillatory Mode**	**Lateral Oscillatory Mode**
16Hz	1.1765Hz	0.6993Hz

As discussed in Section III, if the flapping frequency is ten times higher than the frequencies of the natural modes, the quasi-static approximation works well. Apparently, from the frequencies comparison in **TABLE IX**, the flapping frequency is at least 13 times the natural frequencies. Hence, the cycle-averaged model is valid.

VI. CONCLUDING REMARKS

Cycle-averaged linear longitudinal and lateral models of a bi-flap flapping wing platform called the Svari are derived and the derivatives of the models are identified by experimental method. The linear models are about the equilibrium hovering condition.

Stability analysis shows that the Svari platform is unstable at hovering both longitudinally and laterally. The longitudinal natural modes include a short period unstable oscillatory mode, a fast subsidence mode, and a slow divergent mode. The lateral natural modes include a neutral mode, a fast subsidence mode, and a long period unstable oscillatory mode. The quickest t_{double} of the unstable modes is 0.11s equivalent to 1.76 flapping cycles, which is very quick in terms of human reflexes. That means the platform is not possible to be controlled manually by human at hovering equilibrium.

The force and moment measurement fitted nicely to linear curves, proving that the linearization by small perturbation theory is legitimate. The flapping frequency is at least 13 times the natural frequencies, proving that the cycle-averaged model is legitimate.

Future work shall include the identification of the rate derivatives, design of a more rigid structure for experiment purposes, and construction of nonlinear model.

ACKNOWLEDGEMENT

Authors appreciate the financial support from Future System and Technology Directorate of Singapore (Programme No. PA 9011102539) and Fluid Mechanics Laboratory of Mechanical Engineering Department, National University of Singapore. The authors would also like thank the other student team members who originally designed the Svari platform. They are Mr. Lu Weiyao, Mr. See Jun Hong Mason, Mr. Tan Wei Han Gerald, and Mr. Quek Chen Hua.

REFERENCES

[1] D. B. Doman, M. W. Oppenheimer, and D. O. Sigthorsson, "Dynamics and control of a minimally actuated biomimetic vehicle: part I – aerodynamic model," presented at 2009 AIAA Guidance, Navigation, and Control Conference, Chicago, IL.

[2] X. Deng, L. Schenato, W. C. Wu, and S. Sastry, "Flapping flight for biomimetic robotic insects part I: system modelling," *IEEE Transaction on Robotics*, volume 22, number 4, 2006, pp. 776-788. CrossRef

[3] Z. A. Khan, S. K. Agrawal, "Control of longitudinal flight dynamics of a flapping-wing micro air vehicle using time-averaged model and differential flatness based controller," in *Proc. American Control Conference*, New York, 2007, pp. 5284–5289.

[4] M. Sun, J. Wang, and Y. Xiong, "Dynamic flight stability of hovering insects," *Acta Mechanica Sinica*, volume 23, number 3, 2007, pp. 231-246. CrossRef

[5] G. K. Taylor and A. L. R. Thomas, "Animal flight dynamics II. Longitudinal stability in flapping flight," *Journal of Theoretical Biology*, volume 214, 2002, pp. 351-370. CrossRef

[6] M. Sun and Y. Xiong, "Dynamic flight stability of a hovering bumblebee," *The Journal of Experimental Biology*, volume 208, 2005, pp. 447-459. CrossRef

[7] N. Xu and M. Sun, "Lateral dynamic flight stability of a model bumblebee in hovering and forward flight," *Journal of Theoretical Biology*, volume 319, 2013, pp. 102-115. CrossRef

[8] N. Gao, H. Aono, H. Liu, "A numerical analysis of dynamic flight stability of hawkmoth hovering," *Journal of Biomechanical Science and Engineering*, volume 4, number 1, pp. 105–116, 2009. CrossRef

[9] N. Gao, H. Aono, H. Liu, "Perturbation analysis of 6DoF flight dynamics and passive dynamic stability of hovering fruit fly *Drosophila melanogaster*," *Journal of Theoretical Biology*, volume 270, number 1, pp. 98–111, February 2011. CrossRef

[10] I. Faruque, J. S. Humbert, "Dipteran insect flight dynamics. Part 1: longitudinal–directional motion about hover," *Journal of Theoretical Biology*, volume 264, number 2, 2010, pp. 538-552. CrossRef

[11] I. Faruque, J. S. Humbert, "Dipteran insect flight dynamics. Part 2: lateral–directional motion about hover," *Journal of Theoretical Biology*, volume 265, number 3, 2010, pp. 306-313. CrossRef

[12] Y. Zhang, M. Sun, "Dynamic flight stability of a hovering model insect: lateral motion," *Acta Mechanica Sinica*, volume 26, number 2, 2010, pp. 175–90. CrossRef

[13] M. Groen, B. Bruggeman, B. Remes, R. Ruijsink, B. van Oudheusden, and H. Bijl, "Improving flight performance of the flapping wing MAV DelFly II," presented at 2010 International Micro Air Vehicle conference and competitions (IMAV), Braunschweig, Germany.

[14] R. C. Nelson, *Flight stability and automatic control 2nd Edition*. Singapore: McGraw-Hill, 1998, ch. 4.